

Article

Peri-Gondwanan Provenance and Geodynamic Evolution of The Guadaiza Nappe (Alpujarride Complex, Betic Cordilleras, Spain): Insights on The Paleotethyan Paleogeography

José Julián Esteban *, Julia Cuevas and José María Tubía

Department of Geology, Faculty of Science and Technology, University of the Basque Country (UPV/EHU), Apto. 644, 48080 Bilbao, Spain; julia.cuevas@ehu.eus (J.C.); jm.tubia@ehu.eus (J.M.T.)

* Correspondence: jj.esteban@ehu.eus; Tel.: +34-946-01-24-53

Abstract: Based on the LA-ICP-MS U-Pb zircon ages of four metamorphic samples, we discuss the geochronology and provenance of the Guadaiza nappe, an allochthonous unit that underlies the Ronda peridotites (Betic Cordilleras, Spain). The Guadaiza nappe is composed of Triassic marbles overlying a metapelitic sequence with schists and migmatites. Zircons from a quartzite interlayered with the marbles yield a maximum depositional age of ca. 289 Ma that supports the Triassic age. The idiomorphic morphology of these Paleozoic zircon crystals and the lack of late-Variscan metamorphism (ca. 300 Ma) supports a proximal source area, and suggests that the marbles were discordantly deposited over the metapelitic sequence, along the northern margin of the Alboran microplate. The zircon patterns from the metapelitic sequence mainly yield Paleoproterozoic (ca. 1.6–2.5 Ga), Tonian–Stenian (ca. 1000 Ma), Ediacaran–Cryogenian (ca. 600 Ma) and Paleozoic (ca. 500 Ma) age clusters. These results suggest provenance from areas within the triangle bound by the West African Craton, the Metasaharan Craton and the Hun Superterrane during the Paleotethys opening (Silurian–Devonian). A Silurian–Carboniferous deposition age for the schist protoliths is constrained by the youngest detrital zircon population (ca. 443 Ma) and the Variscan age of their migmatization by an additional peak of around 299 Ma in the migmatites.

Keywords: peri-Gondwana; Betic Cordilleras; Guadaiza nappe; detrital zircon; LA-ICP-MS



Citation: Esteban, J.J.; Cuevas, J.; Tubía, J.M. Peri-Gondwanan Provenance and Geodynamic Evolution of The Guadaiza Nappe (Alpujarride Complex, Betic Cordilleras, Spain): Insights on The Paleotethyan Paleogeography. *Minerals* **2022**, *12*, 325. <https://doi.org/10.3390/min12030325>

Academic Editors: Victoria B. Ershova, Artem V. Moiseev, Andrey Khudoley and Manuel Francisco Pereira

Received: 20 January 2022

Accepted: 3 March 2022

Published: 5 March 2022

Publisher's Note: MDPI stays neutral with regard to jurisdictional claims in published maps and institutional affiliations.



Copyright: © 2022 by the authors. Licensee MDPI, Basel, Switzerland. This article is an open access article distributed under the terms and conditions of the Creative Commons Attribution (CC BY) license (<https://creativecommons.org/licenses/by/4.0/>).

1. Introduction

In the last decade, the technological improvement of the geochronological techniques (LA-ICP-MS, SHRIMP, SIMS, among others) and the facilities to acquire individual zircon data from sedimentary and metamorphic rocks, as the U-Pb age determination can supply the maximum depositional age or the tectonothermal events, means they have become the perfect geological tool to decipher the paleogeographic and geodynamic evolution of ancient terranes. Some of these terranes, such as the Betic Cordilleras, Kabylean, Peloritian and Calabrian belts scattered around the Alboran Sea (western Mediterranean), form the so-called Alboran microplate [1], AlKaPeCa microplate [2], Mesomediterranean terrain [3] or Alboran Domain [4] that drifted away from northern Gondwana during the Paleotethys aperture (Silurian–Devonian). However, although it has been concluded that it conforms to a peri-Gondwanan terrane, e.g., [5–10], the scarcity of geochronological detrital zircon age data, the variable imprint of the Alpine tectonics that erased the vestiges of previous orogenic events, and, in other cases, the fact that the metamorphic rocks that form the basement have been dated as undifferentiated Paleozoic, makes its paleogeographic location still controversial. On this matter, some authors have suggested that during Cambrian and Ordovician times the Alboran microplate should be located in a central position of the Galatian Superterrane (formerly referred to as the Hun Superterrane, [5,11,12]), lying in between the Aquitaine and the intra-Alpine terranes [11,13]. Instead, other authors have

suggested a westernmost starting localization of the Alboran microplate, in direct relationship with the Ossa-Morena (SW Iberian Massif) and Moroccan Meseta terranes [14,15]. Therefore, the acquisition of new geochronological data will help in providing a better understanding of the tectonic evolution of the Alpine orogenic segments that surround the Alboran Sea.

In this work, we present new U-Pb LA-ICP-MS detrital zircon data from four metamorphic samples of the Guadaiza nappe (western Internal Zone of the Betic Cordilleras, Spain), in order to discuss their geochronology and provenance. The presence of two different migmatization events makes the Guadaiza nappe stand out [16,17] as an interesting target to search for the interrelationship between old and new orogenic events. Moreover, the location of the Guadaiza nappe in the Internal Zones under the ultramafic rocks of the Betic and Rif orogens adds additional interest to the explanation of the obtained results in the oldest orogenies (Variscan, Caledonian, etc.) of the western Mediterranean.

2. Geological Setting

The Guadaiza nappe, one of the nappes that forms the western part of the Alpujarride Complex (Internal Zones of the Betic Cordillera), crops out in two main areas (Figure 1): the Albornoque sector and the Guadaiza tectonic window, surrounded by the largest worldwide exposure of subcontinental lithospheric mantle, the Ronda peridotites. Other minor outcrops of Guadaiza nappe are found in the northern part of the studied region, as small tectonic windows or along the thrust contact between the Ronda peridotites and the Triassic limestones (locally marbles) of the Sierra de Las Nieves. The peridotites also rest over some other continental crustal sequences composed mainly of gneisses, metapelites and marbles belonging to the Ojen nappe and Yunqueira Unit.

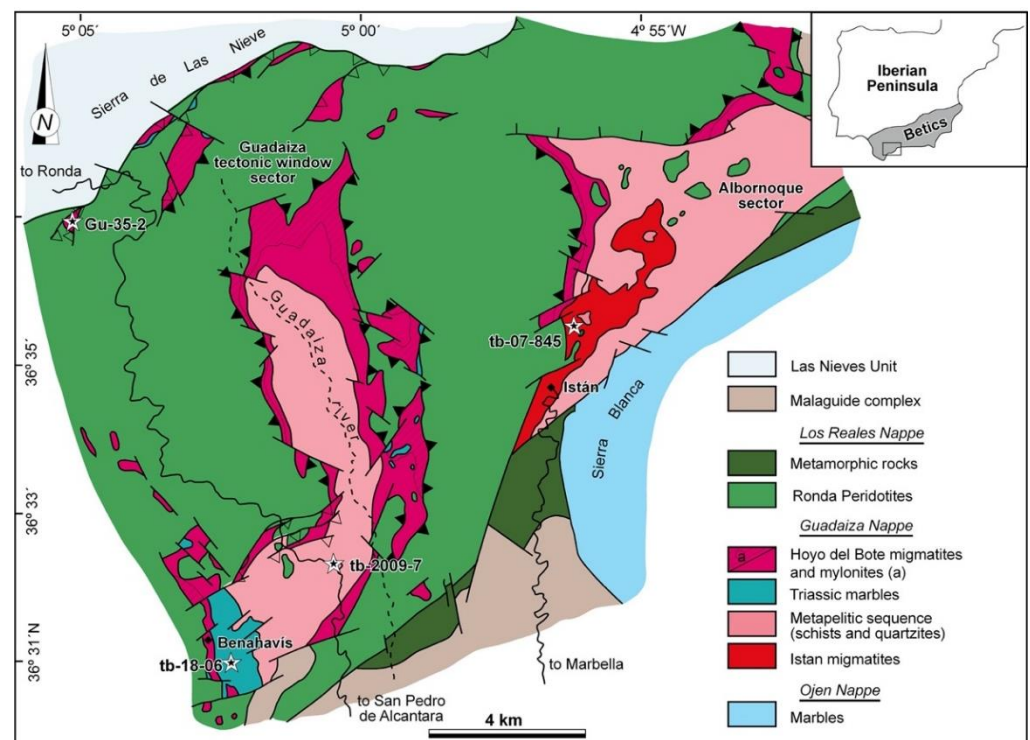


Figure 1. Geological map of the Guadaiza nappe (modified from Esteban et al. [16]) and analysed sample locations (stars).

The lithological sequence of the Guadaiza nappe (Figure 1) is characterized by an undifferentiated Paleozoic metapelitic sequence with interlayered quartzites, schists and minor amphibolites [17]. This sequence is mainly characterized by abundant folded veins of quartz (Figure 2a) and a well-developed axial plane schistosity, S_2 . The metamorphic

conditions of the metapelitic sequence range from the andalusite zone at upper levels to the sillimanite zone close to the underlying Istan migmatites [17]. This member includes gneisses, diatexites, metatexites and medium to fine-grained leucogranites. Over the metapelitic sequence, coarse-grained layered marbles complete the lithological sequence of the Guadaiza nappe. The Triassic age is commonly assigned to these marbles, based on stratigraphic correlations with the less metamorphic Alpujarride units of the eastern Internal Zone of the Betic Cordillera [18,19].

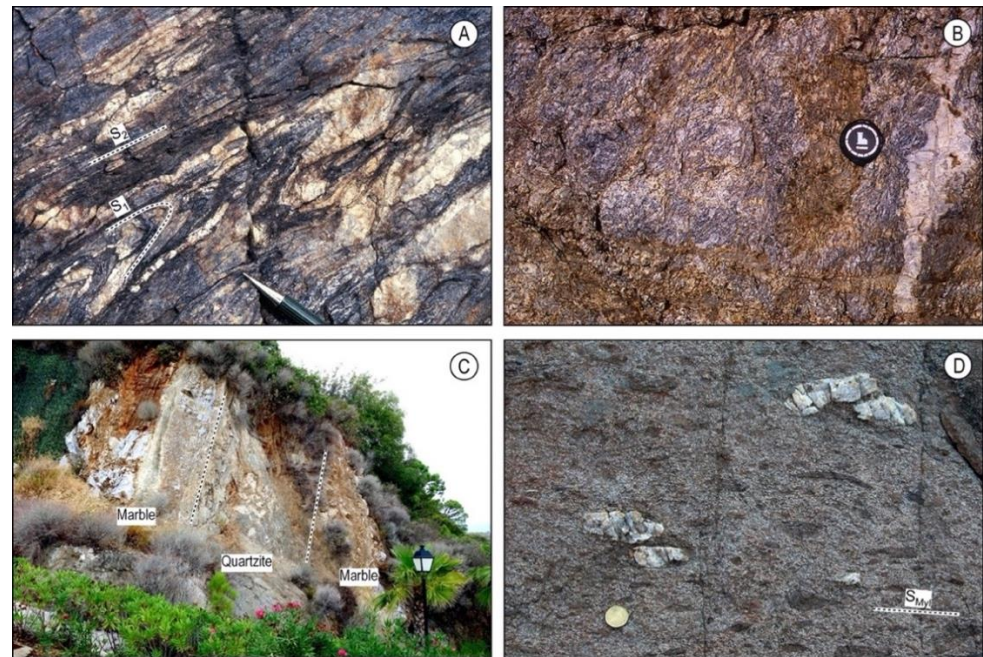


Figure 2. Field images of studied sample outcrops: (A) schists and quartzites of the metapelitic sequence (tb-2009-7), (B) Istan migmatites (tb-07-845), (C) interlayered quartzite within coarse-grained marbles (tb-18-06) and (D) Hoyo del Bote mylonitic migmatite (Gu-35-2) with elongated white quartz nodules and metapelitic restites (dark grey) that define the mylonitic foliation (S_{Myl}).

The Guadaiza nappe shows two main anatexis events recognized from tectonic arguments [17]. The oldest one is recorded by the Istan migmatites (Figure 2b) and is related to the pre-alpine regional metamorphism of the metapelitic sequence. Performed geochronological studies with the $^{207}\text{Pb}/^{206}\text{Pb}$ sequential evaporation technique [20] and U/Pb SHRIMP dating of metamorphic zircons [21] yield Variscan and late-Variscan ages of 319 ± 8 Ma and 299 ± 4 Ma, respectively. The youngest event is represented by the migmatites concentrated around a dynamothermal aureole associated with the emplacement of the overlying Ronda peridotites (Figure 1). This dynamothermal aureole, named as Hoyo del Bote migmatite [17], forms a 100–200-m-thick layer parallel to the lower contact of the peridotite sheet that cuts obliquely all the materials, including the Istan migmatites [16,22] and deflects the previous structures (S_1 , S_2) developed in the metapelitic sequence of the Guadaiza nappe. This dynamothermal aureole is interpreted as a low-viscosity shear zone formed at temperatures high enough, ≈ 725 °C, to promote the partial melting of the underlying metapelitic sequence during the hot emplacement of the Ronda peridotites at Alpine times [23]. It shows an anatexis and strain increase toward the contact to the peridotite slab. Its lower portion contains unfoliated stromatic migmatites that are progressively transformed into nebulitic migmatites rich in rounded blocks of quartz and angular restites from the metamorphic sequence and even the marbles [17]. Toward the peridotites, the coarse-grained and unfoliated migmatites are progressively transformed into protomylonites that give way to S/C mylonites and, finally, ultramylonites. The age of this second migmatization has been constrained by U-Pb SHRIMP dating on zircons at

22 Ma [21] and 22.3 ± 0.7 Ma [23]. Other additional geochronological data come from the granite dykes developed from partial melts arising from the dynamothermal aureole. The granite dykes that intrude into the peridotites also date the anatexis and dynamothermal aureole at around 22 Ma [23,24].

3. Sample Location and Description

Four samples from the Guadaiza nappe (Figure 1) were selected for this study. The samples were collected from the previously described members of the Guadaiza nappe: (1) a schist from the metapelitic sequence (sample tb-2009-7; Figure 2a), (2) a migmatite from the Istan migmatites (sample tb-07-845; Figure 2b), (3) a quartzite interlayered with the coarse-grained Triassic marbles (sample tb-18-06; Figure 2c) and (4) a mylonitic migmatite from the Hoyo del Bote migmatite (sample Gu-35-2; Figure 2d).

The sample tb-2009-7, a fine-grained dark schist located at the upper levels of the metapelitic sequence of the Guadaiza nappe (Figure 1), comes from a strongly deformed zone with a penetrative S_2 -schistosity. S_2 is parallel to the axial plane of tight folds that deform veins of white quartz and an older S_1 -schistosity (Figure 2a), defined by quartz, biotite and graphite. Idioblastic porphyroblasts of andalusite randomly grow on S_2 (Figure 3a).

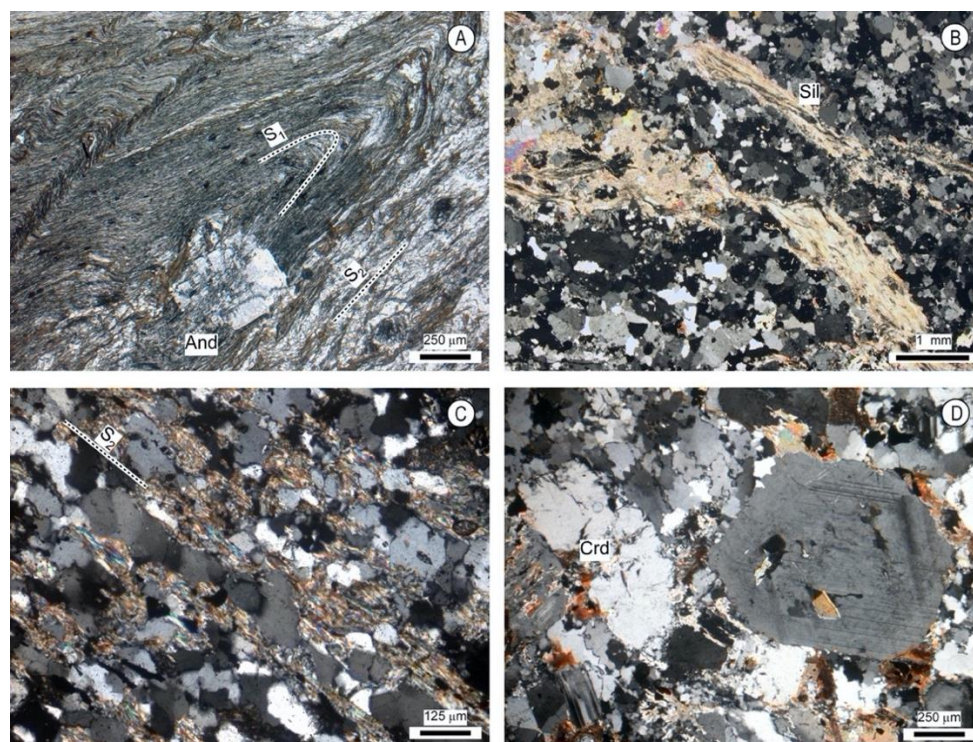


Figure 3. Textural photomicrographs of the analysed samples. (A) Detail of relations in schists between the S_2 parallel to the axial plane of microfolds that deform an older S_1 -schistosity. The schistosity is defined by quartz biotite and graphite. Idioblastic porphyroblast of andalusite (And) growth on S_2 . Plane-polarized light (sample tb-2009-7). (B) Polymineralic sillimanite (Sil) flakes and parallel arrangement of quartz and plagioclase in the sample tb-07-845 from the Istan migmatites. Crossed polars. (C) Microscopic fabric of sample tb-18-06, a quartzite interlayered with marbles, showing a penetrative schistosity, S_2 , marked by the preferred orientation of recrystallized grains of quartz and muscovite. Crossed polars. (D) Idioblastic porphyroblast of plagioclase with inclusions of garnet and biotite. Cordierite (Crd) porphyroblasts and mosaic textures in recrystallized quartz indicate a high temperature deformation of sample Gu-35-2 (Hoyo del Bote migmatite). Crossed polars.

Tb-07-845 is a sample from the Istan migmatites that corresponds to the deepest and most metamorphic zone of the Guadaiza nappe and only crops out in the eastern part of the studied zone (Figure 1). Despite its small areal extent, the Istan migmatites display

great structural diversity, as indicated by the presence of highly differentiated dykes and pods of pegmatite within stromatic or phlebitic migmatite (Figure 2b). These rocks coexist with many restitic zones where sillimanite, biotite and graphite are concentrated. The analysed sample, tb-07-854, shows polymineralic sillimanite flakes that enhance a weak foliation that is defined by the parallel arrangement of slightly elongated grains of quartz and plagioclase (Figure 3b). Interlayered within the coarse-grained marbles that crown the rock sequence of the Guadaiza nappe (Figure 1), the sample tb-18-06 corresponds to a fine-grained quartzite layer about four meters thick (Figure 2c). Both marbles and quartzites show a well-defined foliation, S_2 , related to isoclinal folds. The microscopic fabric exhibits a penetrative schistosity, S_2 , marked by the preferred orientation of recrystallized grains of quartz and muscovite (Figure 3c).

Sample Gu-35-2 belongs to the Hoyo del Bote migmatites that correspond to the dynamothermal aureole formed during the hot thrusting of the Ronda peridotites over the Guadaiza nappe [17]. These migmatites are medium- to coarse-grained diatexite and nebulite that are nearly isotropic and rich in cordierite and feldspar porphyroblasts. They are easily recognizable in the field by the presence of large restitic blocks of white quartz, schist and marbles from the lithological metapelitic sequence of the Guadaiza nappe. Close to the overlying Ronda peridotites, the Hoyo del Bote migmatites have developed a mylonitic foliation, S_{Myl} , that is enhanced by the elongation of the restitic blocks ([22], Figure 2d). The characteristic metamorphic association of these migmatites consists of K-feldspar + plagioclase + biotite + cordierite. The porphyroblasts of K-feldspar usually display poikilitic texture, defined by inclusions of cordierite, quartz, sillimanite, biotite or garnet in random orientation (Figure 3d).

4. Analytical Methods

Zircon crystals were separated by conventional mineral separation techniques (crushing, sieving under 125 μm , heavy liquids and magnetic separation) in the Department of Geology of the University of the Basque Country. Zircon crystals were handpicked aleatory, mounted in epoxy resin and polished approximately to half of their thickness. The internal structure of the zircon crystals was recognized in backscattered electron (BSE) images, obtained using a scanning electron microscope (JEOL7000F-JSM; operative conditions 20 kV, 3 nA and WD 10 mm). Zircon crystals were analysed by LA-ICP-MS at the University of the Basque Country (SGIker-Geochronology and Isotope Geochemistry Facility) using a 193 nm RESOLUTION SE laser with a pulse energy density of $\sim 6 \text{ J cm}^{-2}$ and a frequency of 5 Hz coupled to a Thermo Fisher iCAP Qc quadrupole ICP-MS. The analytical spot size was 30 or 24 μm , depending on zircon size, and in most of the spots the zircon crystals were completely pierced through. Data reduction was carried out using GJ-1 zircon standard for calibration [25] and Plesovice [26] and 91500 zircon [27] as secondary standards (Supplementary Material Table S1). The laboratory staff reduced the data using the Iolite 3.6 software package [28,29] and Vizual Age [30]. Ages in the text and the figures are quoted always with concordance between 90% and 110% and as $^{206}\text{Pb}/^{238}\text{U}$ ages. Tera-Wasserburg diagrams and weighted average ages were produced using Isoplot/Ex 3.0 [31], the distribution of zircon ages and the Kernel Density Estimation (KDE) plots, with bin widths of 60 and 30, respectively, were calculated using DensityPlotter 8.5 [32].

5. LA-ICP-MS Results

5.1. Sample tb-2009-7 (Schist)

Two hundred and one zircon crystals were analysed, of which only one hundred and seventy-four, with Concordia values ranging between 90% and 110%, were considered (Supplementary Material Table S1). Mostly, analysed zircon crystals are xenomorphic and display rounded morphologies (Figure 4). BSE images shows zircon crystals with single and composite structure (cores overgrown by rims). The cores display rounded, eroded and resorbed morphologies with mostly structureless or patchy zonings, while the rims display oscillatory and homogenous zoning. Single zircon crystals have oscillatory

and mainly homogenous zonings. Measured Th/U ratios are between 1.71 and 0.01. Mostly, zircons display Th/U ratios > 0.1 ($n = 163$) and only 11 zircon analyses have Th/U ratios < 0.1 ($n = 11$) (Figure 5).

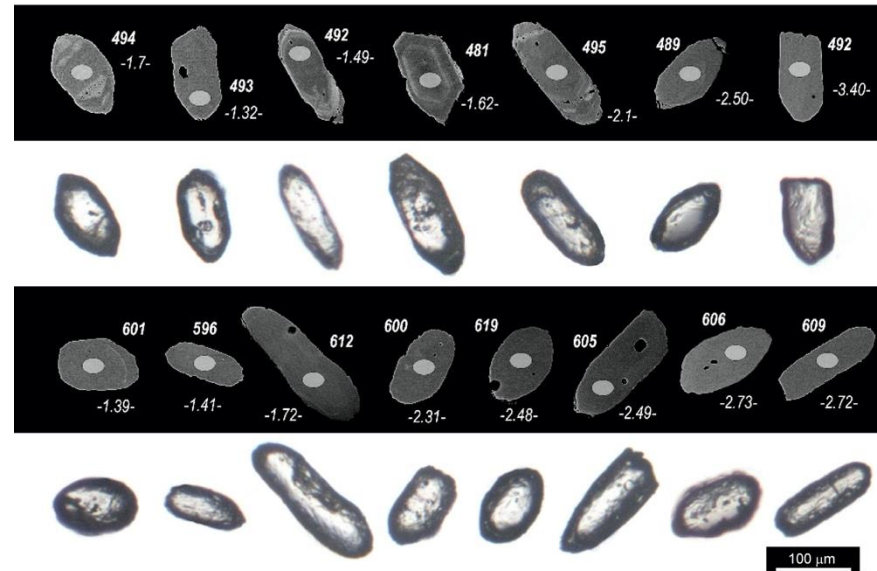


Figure 4. Backscattered electron images and optical photomicrographs of analysed zircons from tb-2009-7 sample (schist). Ellipses mark analytical spot locations and the text shows spot names (italics) and $^{208}\text{Pb}/^{236}\text{U}$ age in Ma (bold).

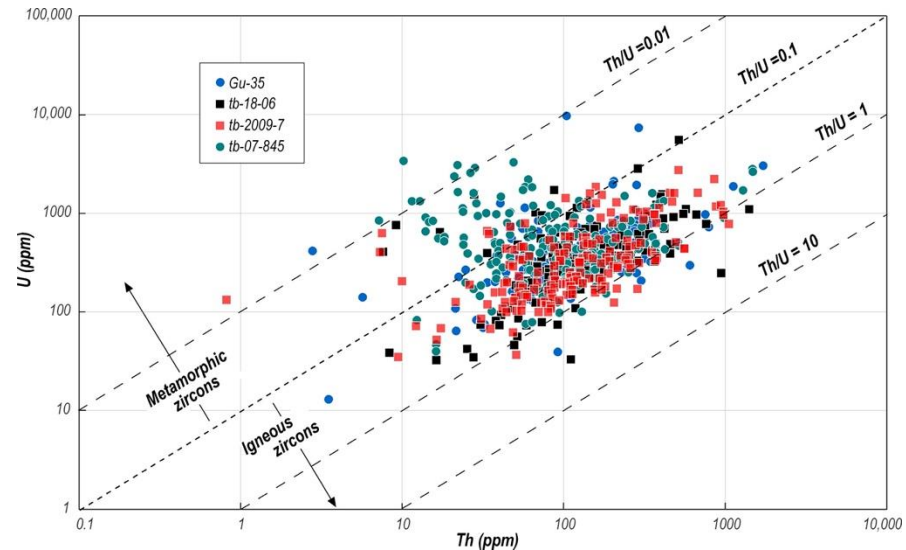


Figure 5. U vs. Th compositional diagram of analysed zircons.

Although age distribution patterns of the analysed zircons are scattered from 256 to 2704 Ma (Figure 6a), about 79% of them yield Precambrian ages that mostly group around Neoproterozoic (50%; ca. 551–998 Ma) and Paleoproterozoic (20%; ca. 1.6–2.5 Ga) peaks, with minor Mesoproterozoic (6%; ca. 1.0–1.1 Ga) and Archean (3%; ca. 2.5–2.7 Ga) populations. The remaining 21% analyses correspond to Paleozoic ages. Three main populations can be peaked from KDE plots at ~ 500 Ma, ~ 600 Ma and ~ 1 Ga (Figure 6a). The calculated weighted average $^{206}\text{Pb}/^{238}\text{U}$ ages of the populations result in mean values of 494 ± 3 Ma ($n = 8$), 599 ± 3 Ma ($n = 13$) and 1010 ± 5 Ma ($n = 6$). A weighted mean age of 443 ± 4 Ma arising from the youngest four zircon crystals can be considered as the

youngest zircon population. Th/U analyses with values < 0.1 are mainly concentrated around the zircon age population of ~600 Ma (Figure 7).

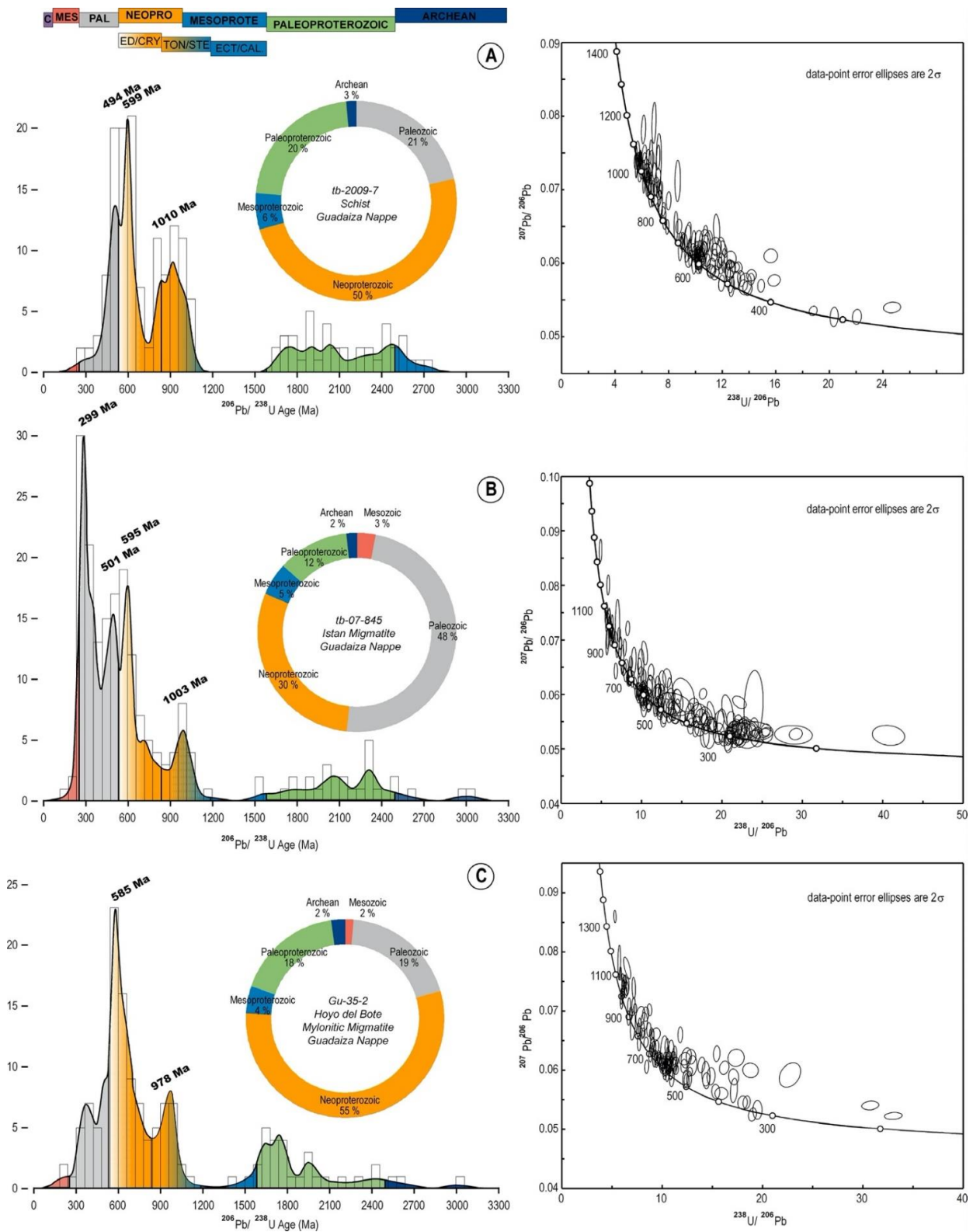


Figure 6. Tera-Wasserburg, Kernel Density Estimation (KDE) plots and histograms of age distributions of analysed zircons of Guadaiza's samples. (A) tb-2009-1, (B) tb-07-845 and (C) Gu-35-2.

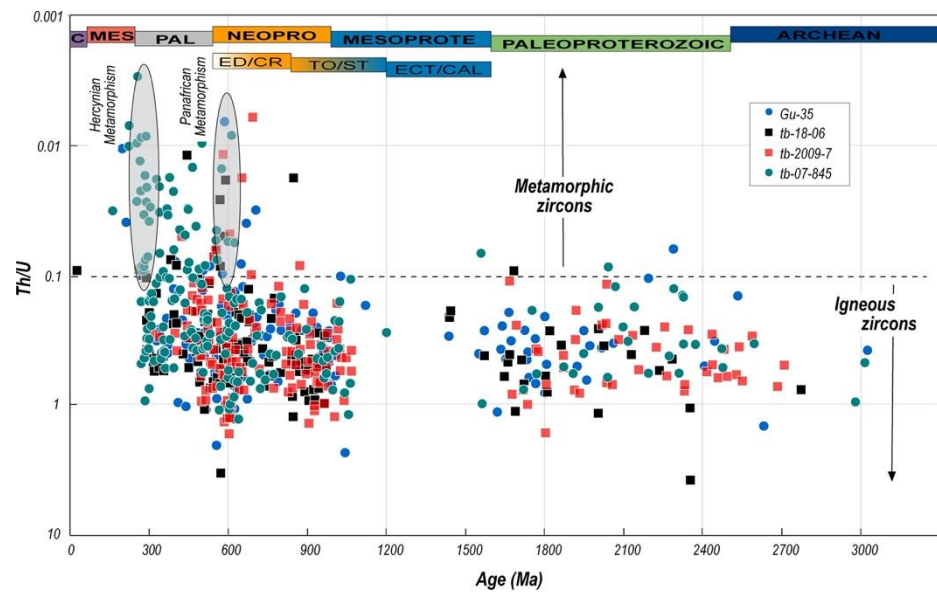


Figure 7. Th/U vs. $^{206}\text{Pb}/^{238}\text{U}$ Age (Ma) of analysed zircons of Guadaiza nappe’s samples.

5.2. Sample *tb-07-845* (Istan Migmatite)

Two hundred and forty-seven zircons were analysed by LA-ICP-MS and only one hundred and ninety-four yielded concordant ages between 156 Ma and 3009 Ma (Supplementary Material Table S1). Analysed zircon crystals are idiomorphic and display prismatic or bipyramidal morphologies (Figure 8). Most of the zircons display a composite core–rim structure. The composite zircons have an eroded or resorbed detrital inclusions-free core overgrown by a lighter and a concentric poikilitic rim structure (Figure 8). Single zircon crystals display mainly continuous oscillatory or homogenous zonings. Although the measured Th/U ratios vary widely between 1.312 and 0.01 (Figure 5), most analyses (n = 142) yield Th/U ratios >0.1 and 52 zircon analyses have Th/U ratios < 0.1.

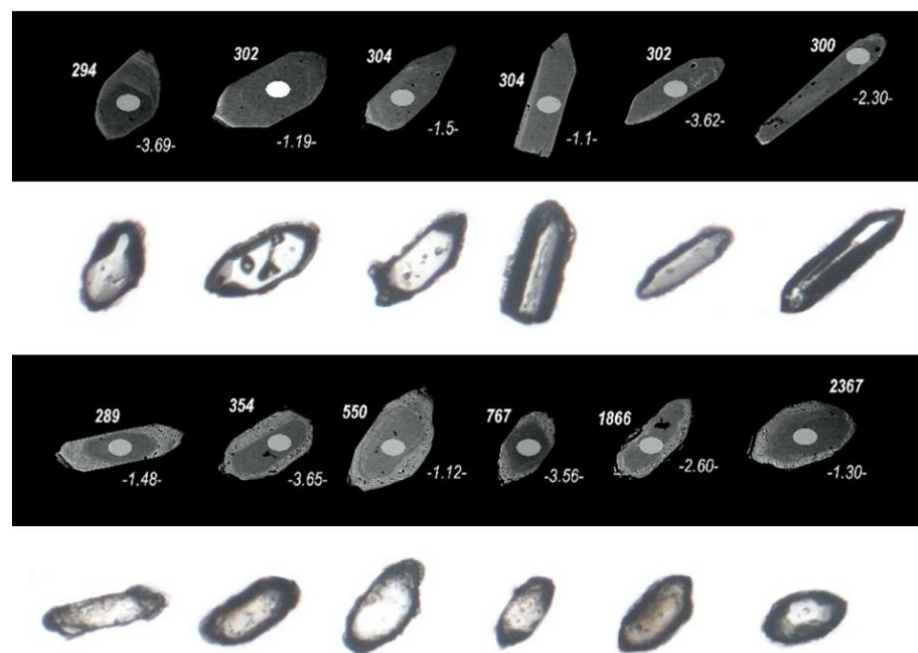


Figure 8. Cont.

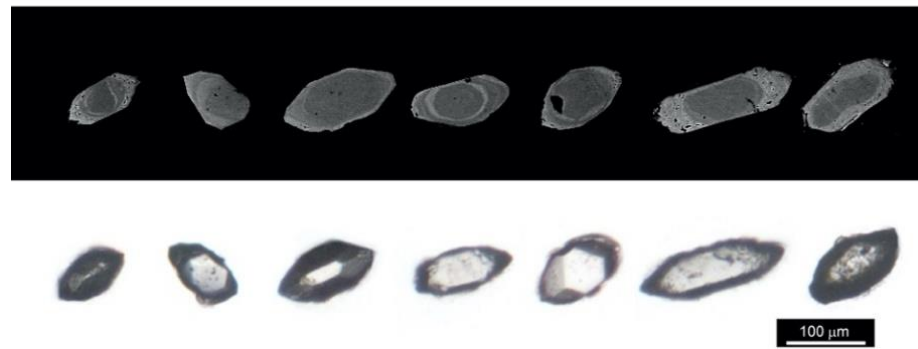


Figure 8. BSE images and optical photomicrographs of analysed zircons from tb-07-845 sample (migmatite). Ellipses mark analytical spot locations and the text shows spot names (*italics*) and $^{208}\text{Pb}/^{236}\text{U}$ age in Ma (**bold**).

Age distribution patterns (Figure 6b) show that 48% of the analysed zircons are Paleozoic and that 3% have a Mesozoic origin. There are 49% that are Precambrian in age and mostly yield Neoproterozoic (30%; ca. 548–998 Ma) and Paleoproterozoic (12%; ca. 1.7–2.5 Ga) ages, with the rest being Mesoproterozoic (5%; ca. 1.0–1.6 Ga) and Archean (2%; 2.6–3.0 Ga). Four main populations are peaked at ~300 Ma, ~500 Ma, ~600 Ma and ~1 Ga (Figure 6b). The calculated weighted average $^{206}\text{Pb}/^{238}\text{U}$ ages of the populations raises values of 299 ± 2 Ma ($n = 10$), 500 ± 4 Ma ($n = 9$), 595 ± 4 Ma ($n = 13$) and 1003 ± 9 Ma ($n = 6$). Th/U analyses with values < 0.1 are concentrated within ~300 and ~600 Ma aged zircon populations (Figure 7).

5.3. Sample Gu-35-2 (Hoyo Del Bote Migmatite)

One hundred and seventy-five zircons were analysed by LA-ICP-MS. As in the Is-tan migmatite sample, the analysed zircon crystals are idiomorphic and display mainly bipyramidal morphologies (Figure 9). Single and composite core–rim structure zircons are observed. The crystals with composite structure have eroded and resorbed cores and sometimes are overgrown by a light and thin rim. Due to their thinness these rims could not be dated by LA-ICP-MS. Measured Th/U ratios are in between 2.4 and 0.01. Most zircons display Th/U ratios > 0.1 ($n = 128$) and only 13 zircon analyses have Th/U ratios < 0.1 (Figure 5).

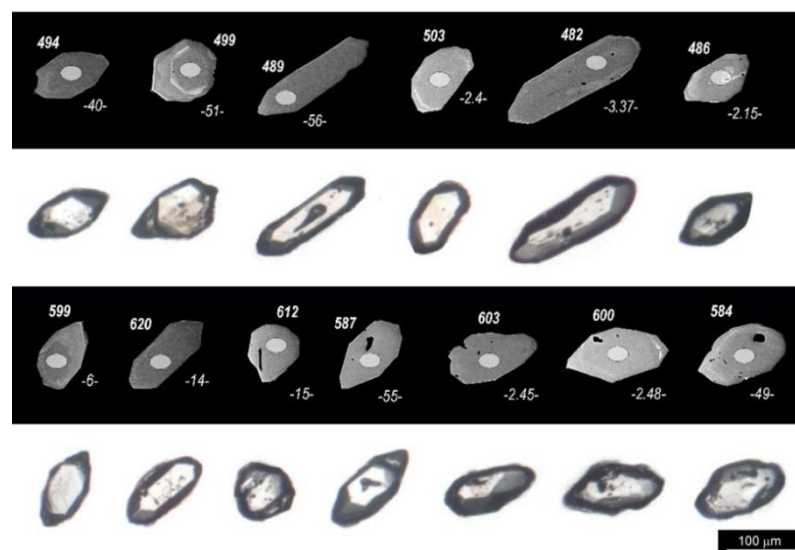


Figure 9. BSE images and optical photomicrographs of analysed zircons from Gu-35-2 sample (mylonitic migmatite). Ellipses mark analytical spot locations and the text shows spot names (*italics*) and $^{208}\text{Pb}/^{236}\text{U}$ age in Ma (**bold**).

Age distribution patterns (Figure 6c) from 192 to 3019 Ma show that 79% of the analysed zircons are Precambrian in age and mostly yield Neoproterozoic (55%; ca. 543–1000 Ma) and Paleoproterozoic (18%; ca. 1.6–2.4 Ga) ages, with the rest being Mesoproterozoic (4%; ca. 1.0–1.6 Ga) and Archean (2%; ca. 2.5–3.0 Ga). The remaining analyses give Paleozoic (19%; ca. 278–524 Ma) or Mesozoic (2%; ca. 192–206 Ma) ages. Two main populations can be peaked at 585 ± 3 Ma ($n = 9$) and 978 ± 7 Ma ($n = 5$). Th/U analyses with values < 0.1 mainly come from the zircon population aged at 585 ± 3 Ma (Figure 7).

5.4. Sample *tb-18-06* (Quartzite Interlayered with Marbles)

One hundred and seventy-two zircon crystals were analysed and only one hundred and thirty-four were considered (Supplementary Material Table S1). While zircon crystals mainly show idiomorphic shapes in the migmatites (Hoyo del Bote and Istan) and xenomorphic in the schists, the zircon crystals in the quartzite of the Guadaiza nappe display both xenomorphic and idiomorphic zircon populations in similar proportions (Figure 10). The xenomorphic zircon population display a composite structure but most are a single structure. The latter display homogenous or oscillatory zonings, whereas those with a composite structure display a rounded or resorbed core with homogeneous or oscillatory zoning overgrown by a thin and lighter rim. Measured Th/U ratios are in between 0.02–3.9 and 0.01–0.56 for the xenomorphic and idiomorphic zircon populations, respectively (Figure 5).

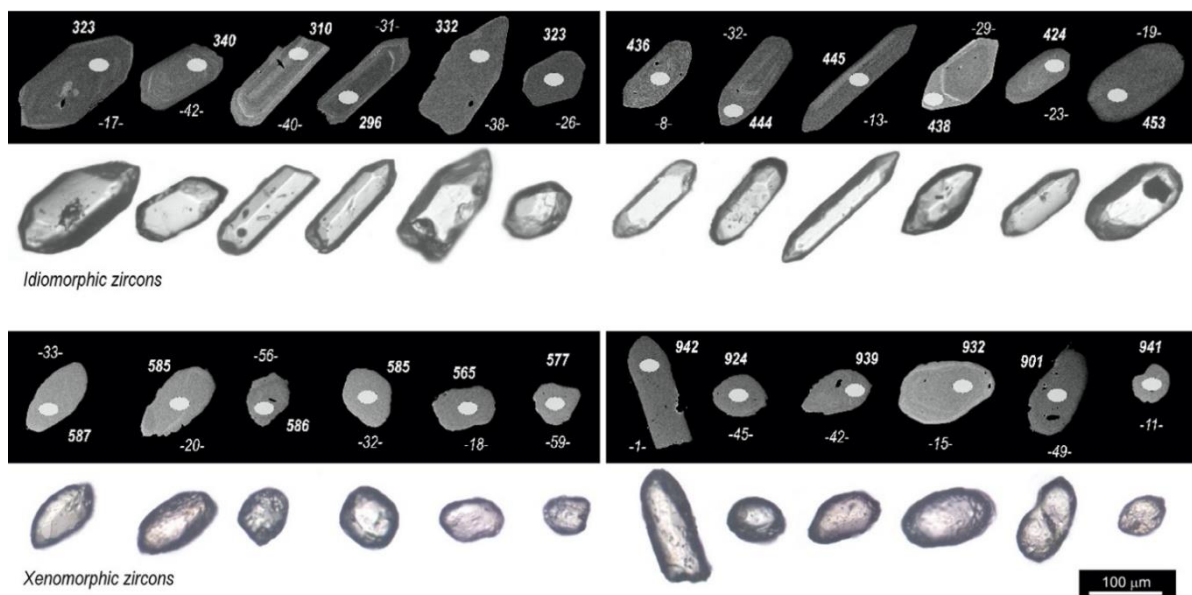


Figure 10. BSE images and optical photomicrographs of analysed zircons from *tb-18-06* sample (quartzite). Ellipses mark analytical spot locations and the text shows spot names (*italics*) and $^{208}\text{Pb}/^{238}\text{U}$ age in Ma (**bold**).

The general age distribution patterns (Figure 11) from 21 to 2768 Ma show that 70% of the analysed zircons are Precambrian in age, Neoproterozoic (52%; ca. 547–967 Ma) and Paleoproterozoic (15%; ca. 1.6–2.4 Ga) mainly, the rest being Mesoproterozoic (2%; ca. 1.4–1.6 Ga) and Archean (1%; ca. 2.8 Ga). The remaining analyses yield Paleozoic (29%; ca. 271–539 Ma) or Cenozoic (1%; ca. 21 Ma) ages. Several populations can be peaked for the xenomorphic (~ 600 Ma and ~ 1 Ga) and idiomorphic zircons (~ 300 Ma and ~ 440 Ma) (Figure 11) with weighted average $^{206}\text{Pb}/^{238}\text{U}$ ages of 323 ± 4 Ma ($n = 4$), 442 ± 7 Ma ($n = 6$), 583 ± 5 Ma ($n = 9$) and 947 ± 10 Ma ($n = 7$) (Figure 11). A detailed observation of Th/U vs. $^{206}\text{Pb}/^{238}\text{U}$ ages of analysed samples agree that the idiomorphic zircons are younger than the xenomorphic ones (Figure 7). The youngest determined age populations for the xenomorphic and idiomorphic zircons are 481 ± 8 Ma ($n = 4$) and 289 ± 4 Ma ($n = 3$), respectively.

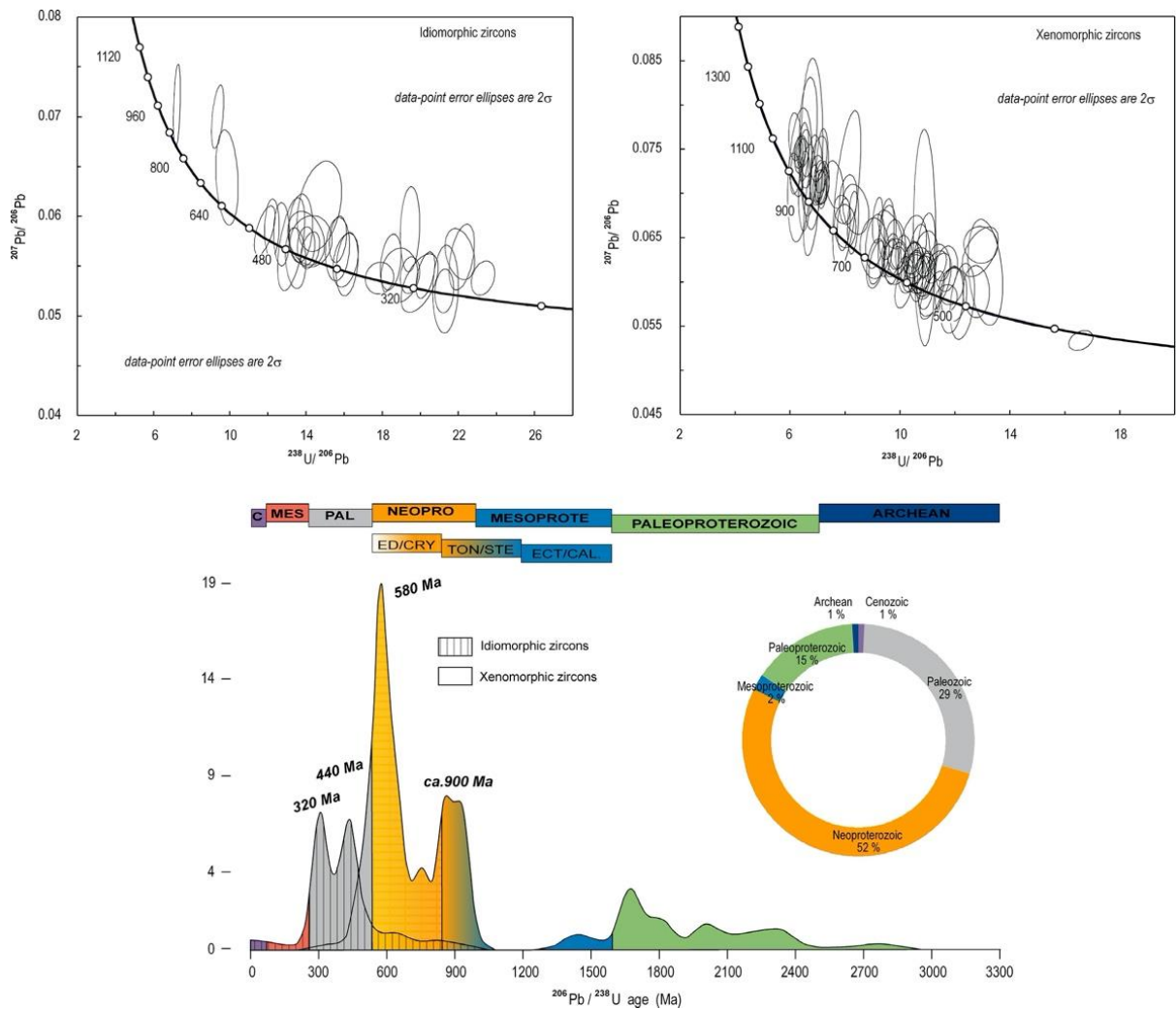


Figure 11. Tera-Wasserburg and KDE age distributions of tb-18-06 sample. Zircon age distribution has been separated according to idiomorphic and xenomorphic zircon morphology.

6. Discussion

6.1. Age of Sedimentation

The interpretation of detrital zircon age populations in metamorphic rocks is often a complex task, as superposed tectonothermal events can disturb the determination of the maximum depositional age of the protoliths. The attempts to place the Guadaiza metapelitic sequence into a paleogeographically reconstructed setting requires at least the following data: (a) the age of the deposition of the sedimentary protoliths, and (b) the age of subsequent events with a thermal input enough to modify the original age record. The maximum depositional age of the pre-Triassic protoliths of the metasedimentary sequence of the Guadaiza nappe is constrained grosso modo by the average of the youngest zircon population (~500 Ma) peaked in the KDE plots (Figure 6a) from the metapelitic sequence and Istan migmatites. A more precise maximum depositional age of 443 ± 4 Ma can be obtained from the weighted average age that defines the youngest zircon population from four zircons of the metapelitic sequence, where the Variscan metamorphism would not lead to the spread of zircon recrystallization. Moreover, the fact that the sample of the Istan migmatites displays a prominent peak at the age ~299 Ma and it fits with that reported by Acosta et al. [33] suggests that it can be considered as being of the age of the late-Variscan metamorphism that led to the anatexis and migmatization of the sequence. Therefore,

at least, a Silurian–Carboniferous age (299–443 Ma) can be predicted for the metapelitic sequence sedimentation.

6.2. Zircon-Forming Events

Additional interesting results of this work can be deduced from the KDE plots obtained from the protolith regarding the distinguishing of several sequential zircon-forming events that would have taken place along the northern Gondwana margin: (1) high proportion of Paleozoic (21%; ca. 256–541 Ma), Ediacaran–Cryogenian (34%; ca. 551–838 Ma), Tonian–Stenian (22%; ca. 852–1063 Ma) and Paleoproterozoic ages (20%; ca. 1.6–2.5 Ga) that define three main zircon populations at ~500 Ma, ~600 Ma and ~1 Ga, and (2) the scarcity of Mesoproterozoic ages (6%; ca. 1.0–1.1 Ga).

The scarcity of Mesoproterozoic ages (6%; ca. 1.0–1.1 Ga) compared to Neoproterozoic ages (50%; ca. 551–998 Ma) and Paleoproterozoic (20%; ca. 1.6–2.5 Ga) is considered a typical signature of the West African Craton. It also excludes the derivation of protoliths from cratons widely affected by the Grenville Orogeny like Laurentia, Baltica, Avalonia and Amazonia, as they commonly show a multi-peak Mesoproterozoic distribution, e.g., [34,35] and references therein. The potential Tonian–Stenian zircon population (~1000 Ma) is accepted to be the East African–Arabian zircon province [36] and can be represented by the Metasaharan Craton or the Arabian Shield. Otherwise, the high proportion of Ediacaran (18%; ca. 551–625 Ma) ages, typical of the north Gondwana, suggest a zircon provenance from multiple source areas such as Cadomian peri-Gondwana terrane generated along the northern periphery of the West African Craton during the Cadomian–Avalonian arc formation or even the Pan-African Trans-Saharan Belts, the Metasaharan Craton, Anti-Atlas and the Tuareg Shield, among others. Finally, the detected Cambrian–Ordovician peak (~500 Ma) fits with the widespread magmatic rifting episode widely recorded in the Iberian massif and other peri-Gondwanan terranes that preceded the opening of the Rheic Ocean [37].

Although subjected to some uncertainties [38], the zircon Th/U ratio is used to discriminate between magmatic (Th/U > 0.1) and metamorphic (Th/U < 0.1) zircons, e.g., [39–41]. However, as examples of metamorphic zircon overgrowths with Th/U values higher than 0.1 or even igneous zircons with values lower than 0.1 have been reported, e.g., [26,42], this type of interpretation must be considered carefully. Most of the obtained Th/U ratios in zircon crystals from the Guadaiza nappe are higher than 0.1 (Figure 5 and Supplementary Material Table S1), which agrees with an igneous origin of the zircon crystals. Only a few zircon crystals linked to the ~600 and ~300 Ma age populations display Th/U values lower than 0.1 suggesting apparent metamorphic origins (Figure 7). The age population of ~300 Ma fits with the Paleozoic (late-Variscan) metamorphic event that has been already evidenced in the Istan migmatites (this work), whereas the Pan-African metamorphic belt of ~600 Ma, widely recognized in the Trans-Saharan belt due to the amalgamation of Gondwana, could be proposed as a hypothetical source of metamorphic zircons.

Therefore, the basin from which the sedimentary protoliths of the pre-Triassic rocks of the Guadaiza nappe derive could be located somewhere within the triangle delimited by the West African Craton, the Metasaharan Craton and the Hun Superterrane during the aperture of the Paleotethys. Based on the scarcity of Ordovician ages that could be linked to the accretion of the Hun Superterrane, the authors of [9] have suggested that the Alboran microplate should be located along the southern passive margin of the Paleotethys Ocean, as part of the European Cimmerian Superterrane. Other authors consider that the Alboran microplate should be part of the south passive margin of the European Hunic Superterrane [11,12]. The new data presented (Supplementary Material Table S1) in this work support the presence of Middle Ordovician ages in the Alboran microplate, but until a well-presented Ordovician peak is detected, the possibility of the Alboran microplate being placed in both passive margins of the Paleotethys remains an open question.

A second paleogeographic implication stands out according to the obtained zircon populations of the sedimentary quartzite. The maximum depositional age of the quartzite is constrained by the age of the youngest zircon detrital population age. The youngest detrital zircon population yield an age of 322 Ma (Carboniferous) that can be more accurately constrained by the youngest zircon population showing an age of 289 Ma (Permian). A Triassic age is commonly accepted for the marbles, based on stratigraphic correlations with the paleontologically-dated limestones, Middle to Upper Triassic [43], from the eastern Alpujarrides. Esteban et al. [9] also established an age of 292 Ma for the maximum depositional age for the marble cover of the Ojen nappe. As is well observed, the quartzites do not display the main peak of ca. ~300 Ma, related to the Variscan metamorphism and migmatization of the Guadaiza Unit. These data support the Triassic limestones being discordantly deposited over a previously structured and metamorphosed Variscan basement. Consequently, the idiomorphic morphology of the zircons could not be attributed to the Variscan metamorphism of the Guadaiza nappe.

Upper Ordovician–Lower Silurian magmatism (440–450 Ma) is widely represented in the Pyrenees, the Catalanian Coastal Ranges, the SE corner of the Central Iberian Zone (El Centenillo area) or the NW of the Galicia Tras-os-Montes (Cabo Ortegal) of the Variscan chain [37]. All these areas could agree with being the source of the detected peak of ca. 440 Ma of the Guadaiza's quartzites. However, similar Upper Ordovician–Lower Silurian ages can also be found in the Calabria–Peloritani arc [44–46] or even in the Kabylies [47], suggesting a multiple source area for the quartzites of the Guadaiza nappe at Triassic time. In the same way, the second detected peak of ca. 330 Ma is not conclusive with the source as it fits with the age of the widespread Variscan magmatism and metamorphism all over the western Mediterranean area. However, the paleogeographic reconstructions situate the Alpine Triassic of the Internal Zones of the Betic Cordilleras, dominated mainly by thick and carbonate platform in succession, in the northern margin of the epicontinental platform of the Alboran microplate [3]. This interpretation agrees with the idiomorphic character of our youngest zircons in the quartzite and their low grade of erosion and transport, pointing to a proximal source area for zircons. Therefore, the Alboran microplate basement agrees with being the proximal zircon source rather than the Iberian plate.

6.3. Age of the Migmatization events

The geochronological studies carried out in the Guadaiza nappe have been mainly focused on (1) the granite dykes derived by the partial melting of the continental crust related to the dynamothermal aureole [23,48], (2) the dynamothermal aureole itself [20,23,49] and (3) the underlying anatectic sequence of Istan migmatites [33].

Although there is wide agreement that migmatization of Istan migmatites took place at ca. 280–290 Ma [33], (this work) the geochronological results using $^{207}\text{Pb}/^{206}\text{Pb}$ sequential evaporation technique [33], U-Pb SIMS [49] and SHRIMP [23] give ages in apparent contradiction for the dynamothermal aureole formation. Meanwhile Acosta [20] reported a Variscan age of 319 ± 8 Ma in a quartz–feldspathic diatexite; Platt and Whitehouse [49] in a leucocratic gneiss and Esteban et al. [23] in a mylonitic gneiss reported Alpine ages of 21.1 ± 0.7 Ma and 22.3 ± 0.7 Ma, respectively. In the same way, the geochronological studies performed on the granite dykes by K-Ar [48] and U-Pb SHRIMP [23] techniques have also yielded ages of ca. 21–22 Ma for their intrusion. Otherwise, the work of Acosta et al. [33] carried out at the Istan migmatites, hundreds of meters away from contact with the overlying Ronda peridotites, has suggested that the anatexis of the metapelitic sequence took place at Variscan time (~280–290 Ma), suggesting a pre-Alpine age for the Ronda peridotite emplacement and the dynamothermal aureole. Nevertheless, these authors, based on regional arguments and previous geochronological data, do not discard the necessity of performing detailed geochronological studies on mylonitized migmatites located at the very contact with the peridotites.

However, these apparent age contradictions can be reconciled with field and structural data showing that: (a) two different migmatizations can be recognized in the Guadaiza

nappe, and (b) the dynamothermal aureole, which cuts obliquely previously structured materials, leads new Alpine zircon growth over Variscan or older zircon crystals. The zircon growth is evidenced by the idiomorphic character of the zircon crystals in the Istan migmatite, where composite zircon is characterized by an eroded or resorbed detrital inclusion-free core overgrown by a lighter and a concentric poikilitic rim structure, and, obviously, in those of idiomorphic rims of the dynamothermal aureole. Therefore, during the emplacement of the peridotites, the metamorphism reached temperatures high enough to promote a second event of partial melting of the metapelitic sequence of the Guadaiza nappe and the resulting neof ormation of new zircon crystals or rims around older zircon cores. However, although the obtained zircon ages from the dynamothermal aureole display similar zircon age distribution as their precursors, the metapelitic sequence and the Istan migmatites, the large spot size (25 to 30 μm) of the LA-ICP-MS technique makes it unsuitable to date properly zircon crystals with narrow rims such as those that are commonly found in samples from the Guadaiza nappe. This inherent limitation of the LA-ICP-MS technique implies that other microbeam techniques should be additionally considered in further works.

7. Conclusions

The first U-Pb LA-ICP-MS age determinations of zircon extracted from four samples of the cover (tb-18-06) and the basement (Gu-35-2; tb-2009-7; tb-07-845) of the Guadaiza nappe, underlying the Ronda peridotites (Betic Cordilleras), suggest the following deductions:

- (1) The metapelitic basement of the Guadaiza nappe is defined by the wide presence of Paleozoic, Ediacaran–Cryogenian, Tonian–Stenian and Paleoproterozoic zircon ages and the scarcity of Mesoproterozoic and Archean zircon ages that agrees with a basement location somewhere within the West African Craton, the Metasaharan Craton and the Hun Superterrane during the aperture of the Paleotethys.
- (2) The prominent peak at ca. 299 Ma defined mainly in the Istan migmatites is considered as the age of the late-Variscan metamorphism that led to the anatexis and migmatization of the metapelitic sequence.
- (3) The age of the undifferentiated Paleozoic basement of Guadaiza can be reassigned as Silurian–Carboniferous.
- (4) The maximum age of sedimentation, ca. 289 Ma, and the idiomorphic morphology of Paleozoic zircon crystals of the studied quartzites interlayered with Triassic marbles, suggest a proximal source area for the zircons of the cover of the Guadaiza nappe. Therefore, the Alboran microplate basement agrees with being such a proximal zircon source rather than the Iberian plate. The paleogeographic reconstructions situate the Triassic of the Internal Zones of the Betic Cordilleras in the northern margin of the epicontinental platform of the Alboran microplate.
- (5) The emplacement of the Ronda peridotites promoted zircon recrystallization in the Istan migmatites some tens of meters away from the dynamothermal aureole at Alpine times (ca. 21 Ma).

Supplementary Materials: The following supporting information can be downloaded at: <https://www.mdpi.com/article/10.3390/min12030325/s1>, Table S1: LA-ICP-MS analytical results from studied samples.

Author Contributions: Conceptualization, J.J.E., J.C. and J.M.T.; methodology, J.J.E.; software, J.J.E.; validation, J.J.E., J.C. and J.M.T.; formal analysis, J.J.E.; investigation, J.J.E., J.C. and J.M.T.; data curation, J.J.E.; writing—original draft preparation, J.J.E. and J.C.; writing—review and editing, J.M.T.; visualization, J.J.E.; supervision, J.M.T.; project administration, J.C.; funding acquisition, J.C. All authors have read and agreed to the published version of the manuscript.

Funding: This research was funded by Ministerio de Economía, Industria y Competitividad/Agencia Estatal de Investigación/Fondo Europeo de Desarrollo Regional, European Union, grant number CGL2017-82976-P and Grupos de Investigación, University of the Basque Country, grant number GIU20/017.

Conflicts of Interest: The authors declare no conflict of interest.

References

1. Andrieux, J.; Fontboté, J.M.; Mattauer, M. Sur un modèle explicatif de l'Arc de Gibraltar. *Earth Planet. Sci. Lett.* **1971**, *12*, 191–198. [[CrossRef](#)]
2. Bouillin, J.P.; Durand-Delga, M.; Olivier, P. Betic-Rifian and Tyrrhenian arcs: Distinctive features, genesis and development stages. In *The Origin of Arcs*; Wezel, F.C., Ed.; Elsevier: Amsterdam, The Netherlands, 1986; pp. 281–304.
3. Guerrero, F.; Martín-Algarra, A.; Perrone, V. Late Oligocene–Miocene syn-late-orogenic successions in Western and Central Mediterranean chains from Betic Cordillera to Southern Apennines. *Terranova* **1993**, *5*, 525–544. [[CrossRef](#)]
4. Balanyá, J.C.; García-Dueñas, V. Grandes fallas de contracción y de extensión implicadas en el contacto entre los dominios de Alborán y Sudibérico en el arco de Gibraltar. *Geogaceta* **1986**, *1*, 19–21.
5. Stampfli, G.M.; Borel, G.D. A plate tectonic model for the Paleozoic and Mesozoic constrained by dynamic plate boundaries and restored synthetic ocean isochrones. *Earth Planet. Sci. Lett.* **2002**, *196*, 17–33. [[CrossRef](#)]
6. von Raumer, J.F.; Stampfli, G.M.; Borel, G.; Bussy, F. The organization of pre-Variscan basement areas at the north-Gondwanan margin. *Int. J. Earth Sci.* **2002**, *91*, 35–52. [[CrossRef](#)]
7. Giacommini, F.; Bomparola, R.M.; Ghezzi, C.; Guldbransen, H. The geodynamic evolution of the Southern European Variscides: Constraints from the U/Pb geochronology and geochemistry of the lower Palaeozoic magmatic-sedimentary sequences of Sardinia (Italy). *Contrib. Mineral. Petrol.* **2006**, *152*, 19–42. [[CrossRef](#)]
8. Micheletti, F.; Barbey, P.; Fornelli, A.; Piccarreta, G.; Delouie, E. Latest Precambrian to early Cambrian U-Pb zircon ages of augen gneisses from Calabria (Italy), with inference to the Alboran microplate in the evolution of the peri-Gondwana terranes. *Int. J. Earth Sci.* **2007**, *96*, 843–860. [[CrossRef](#)]
9. Esteban, J.J.; Tubía, J.M.; Cuevas, J.; Vegas, N.; Sergeev, S.; Larionov, A. Peri-Gondwanan provenance of pre-Triassic metamorphic sequences in the western Alpujarride nappes (Betic Cordillera, southern Spain). *Gondwana Res.* **2011**, *20*, 443–449. [[CrossRef](#)]
10. Williams, I.S.; Fiannacca, P.; Cirrincione, R.; Pezzino, A. Peri-Gondwanan origin and early geodynamic history of NE Sicily: A zircon tale from the basement of the Peloritani Mountains. *Gondwana Res.* **2012**, *22*, 855–865. [[CrossRef](#)]
11. Stampfli, G.M. Tethyan oceans. In *Tectonics and Magmatism in Turkey and the Surrounding Area*; Bozurt, E., Winchester, J.A., Piper, J.D.A., Eds.; Special Publication; Geological Society: London, UK, 2000; Volume 173, pp. 1–23.
12. von Raumer, J.F.; Stampfli, G.M.; Bussy, F. Gondwana-derived microcontinents- the constituents of the Variscan and Alpine collisional orogens. *Tectonophysics* **2003**, *365*, 7–22. [[CrossRef](#)]
13. von Raumer, J.F.; Stampfli, G.M. The birth of the Rheic Ocean—Early Palaeozoic subsidence patterns and tectonic plate scenarios. *Tectonophysics* **2008**, *461*, 9–20. [[CrossRef](#)]
14. Stampfli, G.M.; Hochard, C.; Vêrard, C.; Wilhem, C.; von Raumer, J.F. The formation of Pangea. *Tectonophysics* **2013**, *593*, 1–19. [[CrossRef](#)]
15. von Raumer, J.F.; Stampfli, G.M.; Arenas, R.; Sánchez Martínez, S. Ediacaran to Cambrian oceanic rocks of the Gondwana margin and their tectonic interpretation. *Int. J. Earth Sci.* **2015**, *104*, 1107–1121. [[CrossRef](#)]
16. Esteban, J.J.; Cuevas, J.; Vegas, N.; Tubía, J.M. Deformation and kinematics in a melt-bearing shear zone from the Western Betic Cordilleras (Southern Spain). *J. Struct. Geol.* **2008**, *30*, 380–393. [[CrossRef](#)]
17. Tubía, J.M. Estructura de los Alpujarrides occidentales: Cinemática y condiciones de emplazamiento de las peridotitas de Ronda. Parte I: Características litológicas. *Boletín Geológico Minero* **1988**, *99*, 165–212.
18. Tubía, J.M.; Cuevas, J.; Navarro-Vilá, F.; Álvarez, F.; Aldaya, F. Tectonic evolution of the Alpujarride Complex (Betic Cordillera, southern Spain). *J. Struct. Geol.* **1992**, *14*, 193–203. [[CrossRef](#)]
19. Azañón, J.M.; García-Dueñas, V.; Martínez-Martínez, J.M.; Crespo-Blanc, A. Alpujarride tectonic sheets in the central Betics and similar eastern allochthonous units (SE Spain). *C. R. Acad. Sci. Paris* **1994**, *318*, 667–674.
20. Acosta, A. Estudio de los Fenómenos de Fusión Cortical y Generación de Granitoides Asociados a las Peridotitas de Ronda. Ph.D. Thesis, Granada University, Granada, Spain, 1997.
21. Sánchez-Rodríguez, L. Pre-Alpine and Alpine Evolution of the Ronda Ultramafic Complex and Its Country-Rocks (Betic Chain, Southern Spain): U-Pb SHRIMP Zircon and Fission Track Dating. Ph.D. Thesis, ETH Zurich, Zurich, Switzerland, 1998.
22. Tubía, J.M.; Cuevas, J.; Esteban, J.J. Localization of deformation and kinematic shift during the hot emplacement of the Ronda peridotites (Betic Cordilleras, southern Spain). *J. Struct. Geol.* **2013**, *50*, 148–160. [[CrossRef](#)]
23. Esteban, J.J.; Cuevas, J.; Tubía, J.M.; Sergeev, S.; Larionov, A. A revised Aquitanian age for the emplacement of the Ronda peridotites (Betic Cordilleras, southern Spain). *Geol. Mag.* **2011**, *148*, 183–187. [[CrossRef](#)]
24. Priem, H.N.A.; Boelrijk, N.A.I.M.; Hebeda, E.A.T.; Oen, I.S.; Verdurmen, E.A.; Verschure, R.H. Isotopic dating of the emplacement of the ultramafic masses in the Serrania de Ronda. *Contrib. Mineral. Petrol.* **1979**, *70*, 103–109. [[CrossRef](#)]

25. Jackson, S.E.; Pearson, N.J.; Griffin, W.L.; Belousova, E.A. The application of laser ablation inductively coupled plasma mass spectrometry to in situ U-Pb zircon geochronology. *Chem. Geol.* **2004**, *211*, 47–69. [[CrossRef](#)]
26. Sláma, J.; Košler, J.; Condon, D.J.; Crowley, J.L.; Gerdes, A.; Hanchar, J.M.; Horstwood, M.S.; Morris, G.A.; Nasdala, L.; Norberg, N.; et al. Plešovice Zircon—A New Natural Reference Material for U–Pb and Hf Isotopic Microanalysis. *Chem. Geol.* **2008**, *249*, 1–35. [[CrossRef](#)]
27. Wiedenbeck, M.; Alle, P.; Corfu, F.; Griffin, W.L.; Meier, M.; Oberli, F.; von Quadt, A.; Roddick, J.C.; Spiegel, W. 1995. Three natural zircon standards for U–Th–Pb, Lu–Hf, trace element and REE analyses. *Geostand. Newsl.* **1995**, *19*, 1–23. [[CrossRef](#)]
28. Paton, C.; Hellstrom, J.; Paul, B.; Woodhead, J.; Hergt, J. Iolite: Freeware for the visualization and processing of mass spectrometry data. *J. Anal. At. Spectrom.* **2011**, *26*, 2508. [[CrossRef](#)]
29. Paul, B.; Paton, C.; Norris, A.; Woodhead, J.; Hellstrom, J.; Hergt, J.; Greig, A. CellSpace: A module for creating spatially registered laser ablation images within the Iolite freeware environment. *J. Anal. At. Spectrom.* **2012**, *27*, 700–706. [[CrossRef](#)]
30. Petrus, J.A.; Kamber, B.S. VizualAge: A Novel Approach to Laser Ablation ICP-MS U-Pb Geochronology Data Reduction. *Geostand. Geoanalytical Res.* **2012**, *36*, 247–270. [[CrossRef](#)]
31. Ludwig, K.R. *User's Manual for Isoplot/Ex, Version 3.00, A Geochronological Toolkit for Microsoft Excel*; Berkeley Geochronology Center Special Publication: Berkeley, CA, USA, 2003.
32. Vermeesch, P. On the visualisation of detrital age distributions. *Chem. Geol.* **2012**, *312–313*, 190–194. [[CrossRef](#)]
33. Acosta, A.; Rubatto, D.; Bartoli, O.; Cesare, B.; Meli, S.; Pedrera, A.; Azor, A.; Tajcmanová, L. Age of the anatexis in the crustal footwall of the Ronda peridotites, S Spain. *Lithos* **2014**, *210–211*, 147–167. [[CrossRef](#)]
34. Cambeses, A.; Scarrow, J.H.; Montero, P.; Lázaro, C.; Bea, F. Palaeogeography and crustal evolution of the Ossa-Morena Zone, southwest Iberia, and the North Gondwana margin during the Cambro-Ordovician: A review of isotopic evidence. *Inter. Geol. Rev.* **2017**, *59*, 94–130. [[CrossRef](#)]
35. Szczepanski, J.; Turniak, K.; Anczkiewicz, R.; Gleichner, P. Dating of detrital zircons and tracing the provenance of quartzites from Bystrzyckie Mts: Implications for the tectonic setting of the Early Palaeozoic sedimentary basin developed on the Gondwana margin. *Inter. J. Earth Sci.* **2020**, *109*, 2049–2079. [[CrossRef](#)]
36. Stephan, T.; Kroner, U.; Romer, R.L.; Rösel, D. From a bipartite Gondwanan shelf to an arcuate Variscan belt: The early Paleozoic evolution of northern Peri-Gondwana. *Earth-Sci. Rev.* **2019**, *192*, 491–512. [[CrossRef](#)]
37. Gibbons, W.; Moreno, T. *The Geology of Spain*; The Geological Society: London, UK, 2002; 649p.
38. Harley, S.L.; Kelly, N.M.; Möller, A. Zircon behavior and the thermal histories of mountain chains. *Elements* **2007**, *3*, 25–30. [[CrossRef](#)]
39. Hoskin, P.W.O.; Schaltegger, U. The composition of zircon and igneous and metamorphic petrogenesis. *Rev. Mineral. Geochem.* **2007**, *53*, 27–55. [[CrossRef](#)]
40. Rubatto, D. Zircon: The Metamorphic Mineral. *Rev. Mineral. Geochem.* **2017**, *83*, 261–295. [[CrossRef](#)]
41. Fornelli, A.; Micheletti, F.; Piccarreta, G. Late-Proterozoic to Paleozoic history of the peri-Gondwana Calabria-Peloritani Terrane inferred from a review of zircon chronology. *SpringerPlus* **2016**, *5*, 212. [[CrossRef](#)]
42. Ladenberger, A.; Be'eri-Shlevin, Y.; Claesson, S.; Gee, D.G.; Majka, J.; Romanova, I.V. Tectonometamorphic evolution of the Areskutan Nappe-Caledonian history revealed by SIMS U-Pb zircon geochronology. In *New Perspectives on the Caledonides of Scandinavia and Related Areas*; Corfu, F., Gasser, R., Chew, D.M., Eds.; Special Publication; Geological Society: London, UK, 2014; Volume 390, pp. 337–368.
43. Kozur, H.; Mulder-Blanken, C.W.H.; Simon, O.J. On the Triassic of the Betic Cordilleras (southern Spain), with special emphasis on holothurian sclerites. *Stratigr. Palaeontol.* **1985**, *88*, 83–110.
44. Trombeta, A.; Cirrincione, R.; Corfu, F.; Mazzoleni, P.; Pezzino, A. Mid-Ordovician U-Pb ages of porphyroids in the Peloritani Mountains (NE Sicily): Palaeogeographical implications for the evolution of the Alboran microplate. *J. Geol. Soc. Lond.* **2004**, *161*, 265–276. [[CrossRef](#)]
45. Somma, R.; Navas-Parejo, P.; Martín-Algarra, A.; Rodríguez-Cañero, R.; Perrone, V.; Martínez-Pérez, C. Paleozoic stratigraphy of the Longi-Taormina Unit (Peloritani Mountains, southern Italy). *Stratigraphy* **2013**, *10*, 127–150.
46. Fornelli, A.; Festa, V.; Micheletti, F.; Spiess, R.; Tursi, F. Building an Orogen: Review of U-Pb Zircon Ages from the Calabria-Peloritani Terrane to Constrain the timing of the Southern Variscan Belt. *Minerals* **2020**, *10*, 944. [[CrossRef](#)]
47. Peucat, J.J.; Mahdjoub, Y.; Drareni, A. U-Pb and Rb-Sr geochronological evidence for late Hercynian tectonic and Alpine overthrusting in Kabylia metamorphic basement massifs (northeastern Algeria). *Tectonophysics* **1996**, *258*, 195–213. [[CrossRef](#)]
48. Loomis, M.T. Tertiary mantle diapirism, orogeny and plate tectonics east of the Strait of Gibraltar. *Geol. Soc. Amer. Bull.* **1975**, *89*, 172–180. [[CrossRef](#)]
49. Platt, J.P.; Whitehouse, M.J. Early Miocene high-temperature metamorphism and rapid exhumation in the Betic Cordillera (Spain): Evidence from U-Pb zircon ages. *Earth Planet. Sci. Lett.* **1999**, *171*, 591–605. [[CrossRef](#)]